Nanoscale Advances

ROYAL SOCIETY OF CHEMISTRY

PAPER

View Article Online
View Journal | View Issue

Cite this: *Nanoscale Adv.*, 2024, **6**, 5306

Decisive role of electrostatic interaction in rheological evolution of graphene oxide under ultrasonic fragmentation†

Dongpyo Hong, [a] Matlabjon Sattorov, [bd] Ok Sung Jeon,[a] Se Hun Lee,[a] Gun-Sik Park,*[b] Young Joon Yoo*[a] and Sang Yoon Park *[c]

Received 19th April 2024
Accepted 5th August 2024

DOI: 10.1039/d4na00328d

rsc.li/nanoscale-advances

The aqueous dispersibility and processability of graphene oxide (GO) are pivotal for various applications, including the fluid assembly of macroscopic materials and nanofluidic systems. Despite the widespread utilization of ultrasonic treatment to achieve homogeneous dispersions, the rheological changes of GO during sonication have remained relatively unexplored, leading to conflicting research findings. In this study, we demonstrate that the viscoelastic evolution of GO can significantly differ under ultrasonic fragmentation depending on the balance between repulsion force and attraction force at the initial state before fragmentation. When electrostatic repulsion is in delicate equilibrium with attractive forces, gelation occurs under ultrasonic fragmentation, leading to increased viscosity under sonication. Conversely, when electrostatic repulsion predominates, viscosity decreases during sonication. This study reconciles conflicting observations on the rheological evolution of GO dispersions under ultrasonic fragmentation and provides valuable guidance and insights for the rheological engineering of GO colloidal systems.

Introduction

Graphene oxide (GO) has attracted significant attention primarily due to its cost-effectiveness, mass production capability, and the ability to form a stable aqueous dispersion through electrostatic stabilization resulting from the deprotonation of oxygen functional groups.[1] The excellent aqueous stability of GO enables its processing through various fluid assembly methods, including filtration,[2,3] bar-coating,[4,5] wet-spinning,[6–8] spray-coating,[9] and inkjet printing.[10] Additionally, the applications of GO nanofluids themselves are extensive, encompassing areas such as thermal fluids or sensing applications.

The manipulation of the rheological properties of GO dispersions presents a unique avenue for fine-tuning the structure and, in turn, the corresponding physical characteristics of the nanofluid or processed assemblies.[11–14] For instance, employing techniques such as wet spinning and blade-coating of liquid crystalline GO yields highly aligned fibers and films, respectively, where the shear-induced alignment depends on its viscosity.[4] Meanwhile, the formation of GO hydrogels generally results in highly interlocked, porous structures.[15–17] On the other hand, in nanofluidics applications, the viscosity of a GO dispersion has been found to be directly related to the stability and thermal transport properties of the dispersion.[18,19] Therefore, understanding these GO rheological properties, relying on concentration, nanosheet size, and inter-sheet interactions, and expanding engineering methods are essential to tailor the rheological properties of GO to suit various applications.

In general, the viscosity of a GO aqueous dispersion increases with concentration, but an isotropic–nematic transition to a liquid crystalline phase can lead to a partial decrease in viscosity.[12,13] Moreover, previous investigations have revealed that smaller GO nanosheets exhibit lower viscosity, aligning with Newtonian fluid behavior, as predicted by the Maron–Pierce model.[11,20] Even at high concentrations (~10–20 mg mL^{-1}), a similar trend has been consistently reported, attributed to the concept of rotational restriction.[21]

However, when GO dispersions undergo ultrasonication, viscosity occasionally increases, despite the typical fragmentation of the nanosheets. Some studies have posited that this phenomenon arises from the reinforcement of attractive forces between nanosheets due to the creation of fresh edges without oxygen termination, suggesting a potential additive-free method for forming GO hydrogels.[22,23] Nevertheless, despite the ubiquitous use of sonication for achieving homogeneous

[a]*Advanced Institute of Convergence Technology, Seoul National University, Suwon-si 16229, Republic of Korea. E-mail: youngjoonyoo@snu.ac.kr*

[b]*Center for THz-Driven Biomedical Systems, Department of Physics and Astronomy, Institute of Applied Physics, College of Natural Sciences, Seoul National University, Seoul-si 08826, Republic of Korea. E-mail: gunsik@snu.ac.kr*

[c]*School of Electronics Engineering, Kyonggi University, Suwon-si 16227, Republic of Korea. E-mail: yoonpark@kyonggi.ac.kr*

[d]*Seoul-Teracom, Inc., Advanced Institute of Convergence Technology, Suwon-si 16229, Republic of Korea*

† Electronic supplementary information (ESI) available. See DOI: https://doi.org/10.1039/d4na00328d

GO dispersions, observations of fragmentation-induced gelation are scarce, and some studies even pointed out that there was no such gelation.[24,25] These divergent research findings suggest that fragmentation-induced gelation is not a universal phenomenon for general GO dispersion, implying the presence of an underlying constraint.

In this study, we demonstrate whether fragmentation-induced gelation that occurs highly depends on the surface charge of dispersed GO nanosheets. To confirm this, we independently synthesized two types of GO: highly oxidized graphene oxide (HOGO), having a large zeta potential due to its abundance in oxygen functional groups and exhibiting liquid crystallinity, and less oxidized graphene oxide (LOGO), possessing a small zeta potential due to its lack of oxygen functional groups. Interestingly, even in similar size ranges after prolonged fragmentation, HOGO and LOGO showed opposite viscosity trends under sonication, and only GO with a small zeta potential was confirmed to experience fragmentation-induced gelation. Furthermore, by reducing the zeta potential of HOGO through ionic strength, it was confirmed that fragmentation-induced gelation similar to LOGO occurred. Through these results, we were able to conclude that fragmentation-induced gelation can occur only when the attractive and repulsive forces are in close balance (zeta potential ~ -30 mV), while the viscosity of GO with a larger zeta potential keeps decreasing under the same sonication.

Experimental

Materials

H_2SO_4 (95%, EP grade), H_2O_2 (30%, EP grade) and $KMnO_4$ (99.3%, EP grade) were purchased from Daejung Chemicals (Republic of Korea). HNO_3 (95%, GR grade) was purchased from Samchun Chemicals (Republic of Korea). $K_2S_2O_8$ (99%), P_2O_5 (98.5%) and graphite (100 mesh) used for HOGO synthesis were purchased from Sigma-Aldrich (Germany). Graphite (325 mesh) used for LOGO synthesis was purchased from Bay Carbon (USA).

LOGO synthesis

Graphite (1.4 g) was stirred in H_2SO_4 (95%, 70 mL), and $KMnO_4$ (4.2 g) was gradually added to the solution while maintaining a temperature below 10 °C using a chiller bath. The mixture was stirred at 35 °C for 3.5 hours in a water bath. To dilute the resulting mixture, DI water (70 mL) was slowly added under vigorous stirring, ensuring that the temperature remained below 50 °C. The suspension was further treated with H_2O_2 (30%, 3.5 mL) under vigorous stirring. Subsequently, 2 L of water was added to the mixture, and after precipitation, the supernatant was discarded. The precipitated dispersion was purified by repeated centrifugation with additional water until the pH of the mixture reached 6. The resulting precipitate was collected and diluted to a concentration of 16 mg mL^{-1} for the entire investigation.

HOGO synthesis

Graphite (10 g) was stirred with H_2SO_4 (95%, 150 mL) and HNO_3 (95%, 50 mL) for 24 hours, followed by neutralization and repeated cleaning cycles (6 times). The dried graphite intercalated compounds were irradiated with microwaves for 5 seconds to create expanded graphite. The expanded graphite powder (2.1 g), $K_2S_2O_8$ (2.1 g), and P_2O_5 (3.1 g) were added to H_2SO_4 (95%, 200 mL) and stirred for 4.5 hours at 80 °C. The mixture was then poured slowly into 2 L of deionized (DI) water at a temperature lower than 25 °C to collect the solid by filtration. The resulting solid was dried at 60 °C for 12 hours and then added to 200 mL of concentrated H_2SO_4 (95%, 400 mL). KMnO4 (15 g) was slowly added to the mixture after stirring for 24 hours. Subsequently, 1.6 L of water was slowly added under stirring, and H_2O_2 (30%) was dropwise added. The mixture underwent repeated washing by centrifugation until the pH of the supernatant reached 6. The precipitate was collected and diluted to a concentration of 16 mg mL^{-1} for the entire investigation.

Ultrasonic fragmentation of GO

The as-prepared GO dispersions were diluted to 40 mL of 16 mg mL^{-1} in a 70 mL vessel. The dispersions were vigorously stirred overnight to ensure uniform dispersion. Subsequently, the dispersions were sonicated in an ultrasonic cleaner (POWERSONIC 610, 200 W, 40 kHz, HWASHIN TECH CO. LTD, Korea) for up to 1440 min. To minimize the thermal effect, all ultrasonic treatments were conducted in an ice bath, maintaining the water level at the same level as the dispersion.

Characterization

Aqueous dispersions of GO nanosheets sonicated at different periods of time were drop-cast onto an O_2 plasma treated SiO_2 wafer and dried in an oven prior to scanning electron microscopy measurement for size analysis of GO nanosheets (SEM, AURA200, SERON Technology, Korea). The viscosity of the GO dispersion with increasing sonication time was measured using a viscometer (DV2T viscometer, Brookfield Engineering, U.S.A.) with a cylindrical spindle (LV-05) located at the center of the dispersion at 0.5–50 rpm, with a fixed amount of GO dispersion in a 20 mL vessel. Rheological characterization was performed on an advanced rheometric expansion system (ARES, Rheometric Scientific, U.K.) in frequency-sweep mode. X-ray photoelectron spectroscopy (XPS, AXIS supra+, Kratos, U.K.) and Fourier-transform infrared spectroscopy (FTIR, LUMOS II, Bruker, U.S.A.) data were acquired for the cast-dried GO dispersion. The liquid crystallinity of the GO dispersion was assessed by measuring the birefringence of the dispersion using polarized optical microscopy (POM, BX51TRF, Olympus, Japan). The zeta potential of the GO dispersion was measured using an electrophoretic light scattering spectrophotometer (ELS Z neo, Otsuka Portal, Japan).

Results and discussion

Preparation and characterization of LOGO and HOGO

Depending on the synthesis method, GO nanosheets can exhibit considerable variations in morphology and chemical composition.[26] We synthesized two types of GO with greatly different degrees of oxidation to clearly see the effect of surface

charge on their rheological behavior. Specifically, HOGO and LOGO were prepared through independent synthesis routes, while both types of GO were synthesized based on the modified Hummer's methods. LOGO resulted from a one-step oxidation of graphite, while HOGO was synthesized through a two-step oxidation of expanded graphite (Fig. 1a). The expanded graphite precursor used for HOGO eases the penetration of the intercalation agent and oxidation agent, elevating the degree of oxidation of the final product.[27,28] The difference in the chemical composition of LOGO and HOGO was analyzed through XPS measurements. The C/O ratio estimated from the area of the C 1s peak and O 1s peak in the XPS signal was 2.60 (error: 0.04) for LOGO and 2.17 (error: 0.04) for HOGO, confirming that HOGO contains more oxygen functional groups than LOGO. The higher degree of oxidation in HOGO results from easier infiltration of the excessive oxidation agent into the expanded graphite precursor of HOGO. The differences in the types of oxygen functional groups were analyzed by deconvoluting the XPS C 1s peak, as shown in Fig. 1b. The C 1s peak was deconvoluted into an sp^2 peak at 284.5 eV, an sp^3 peak at 285.1 eV, a C–OH peak at 286.4–286.5 eV, a C–O–C peak at 286.8 eV, a C═O peak at 288–288.1 eV and an O═C–O peak at 288.9–289.3 eV.[29] An asymmetric peak shape was used for fitting the sp^2 peak to account for its intrinsic shape, while a Gaussian peak shape was used for all other peaks.[30,31] The full-width half maximum (FWHM) of the peaks was constrained to a range of 1.2–1.4 eV. When comparing the areas of each peak, HOGO exhibited a higher area for carbon-oxygen bonding peaks relative to the sp^2 and sp^3 peaks (Fig. 1c). This difference was also clearly visible in the color of the dispersion; HOGO appeared more transparent and had a bright, yellowish tint compared to LOGO, which is a characteristic appearance typically seen in highly oxidized GO (Fig. S1†).[12]

These differences in oxygen groups led to significant variations in the surface charge of each GO nanosheet in aqueous dispersions, as the deprotonation of oxygen functional groups such as hydroxyl and carboxyl groups in GO is the origin of the negative surface charge of GO.[1] In the case of HOGO, not only did the peak area of oxygen functional groups increase compared to the sp^2 peak area, but the proportion of C–OH within the oxygen groups also increased. The calculations showed that the overall area ratio of C–OH to the total oxygen group peak was 32% for LOGO, whereas it was 38% for HOGO. Additionally, the proportions of C–O–C and C═O were lower, while the proportion of O═C–O remained consistent. As expected, the zeta potentials measured by ELS were −32 mV for LOGO and −54 mV for HOGO. HOGO exhibited a larger zeta potential due to its richer oxygen groups (Fig. 1c), while both have enough zeta potentials (<−30 mV) for forming a stable dispersion. The average size of the GO sheets measured by SEM was 1.9 μm for LOGO and 5.4 μm for HOGO, indicating that HOGO has a larger size than LOGO (Fig. 1d and e). This is because the full oxidation of the large expanded graphite precursor for HOGO minimizes the size loss due to crack generation during the exfoliation process in water.[32] Therefore, it was confirmed that LOGO has a smaller size, lower oxygen content, and lower surface charge compared to HOGO.

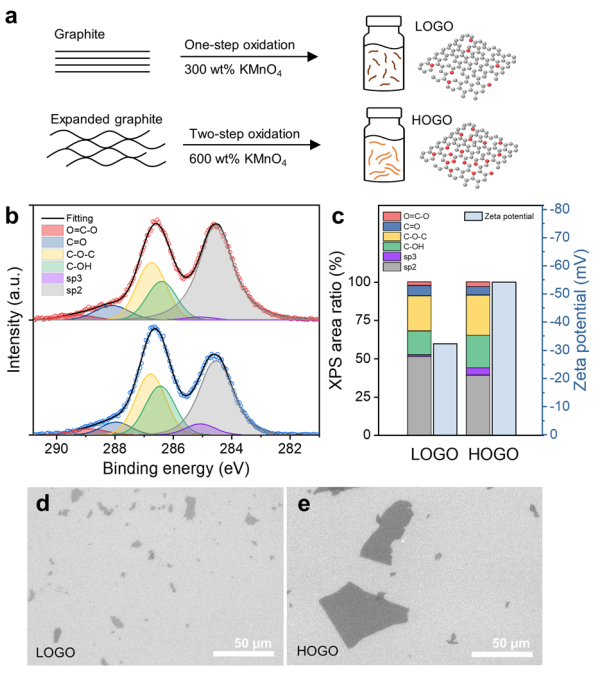

Fig. 1 Synthesis of two distinct types of GO. (a) Schematic for synthesis of LOGO and HOGO. (b) Deconvolution of XPS C 1s spectra. (c) Area ratio of deconvoluted peaks in XPS C 1s and zeta potential. (d and e) SEM images of LOGO and HOGO nanosheets, showing larger lateral size of HOGO than LOGO.

Ultrasonic fragmentation of LOGO and HOGO

In general, when subjected to ultrasonication, GO sheets undergo a process of fragmentation and exfoliation.[33–35] In this section, we focused on understanding how the initial state difference between HOGO and LOGO influences the fragmentation process under ultrasonication. The sizes of more than 500 GO sheet samples were measured by SEM and statistically analyzed at various ultrasonication time points. Fig. 2a and b illustrate the change in the size distribution of GO sheets with ultrasonication time. Even before undergoing ultrasonication, the size distribution of GO sheets for both HOGO and LOGO followed a log-normal distribution. This suggests that the size distribution of initial GO is inherently determined by cracks generated during oxidation or exfoliation processes.[36] At the outset, LOGO showed hardly any GO sheets with sizes exceeding 10 μm, whereas HOGO exhibited relatively large GO sheets, with sizes reaching up to 30 μm. With increasing sonication time, the size distribution of both GO types showed a shift towards smaller sizes, retaining the log-normal shape. Both LOGO and HOGO showed a decrease in average size with increasing ultrasonication time, and when plotted on a log–log scale against time, they exhibited linearity (Fig. 2c). Although the fragmentation behavior of the two GO types did not significantly differ, HOGO displayed a slightly steeper slope of fragmentation. This difference can be attributed to more abundant oxygen functional groups and denser structural defects in HOGO, rendering it more susceptible to fragmentation.[37]

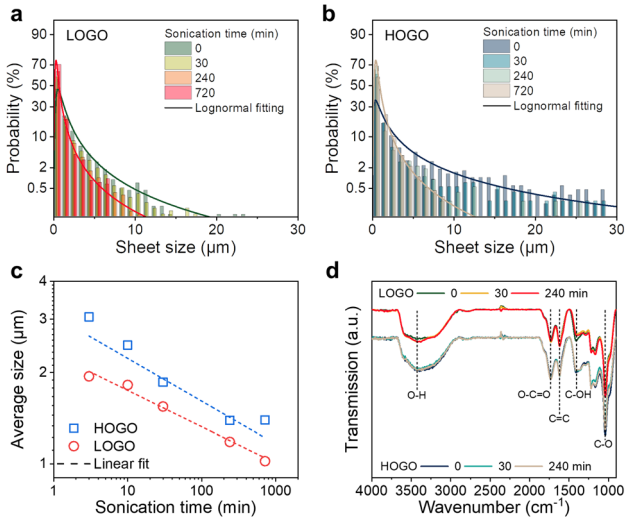

Fig. 2 Analogous ultrasonic fragmentation of LOGO and HOGO. (a and b) GO sheet size distribution measured by SEM of LOGO and HOGO after different times of ultrasonic treatment. Solid lines indicate lognormal fitting of the distributions. (c) Log–log plot of average size *versus* sonication time. (d) FTIR spectra of LOGO and HOGO showing negligible chemical change during bath sonication.

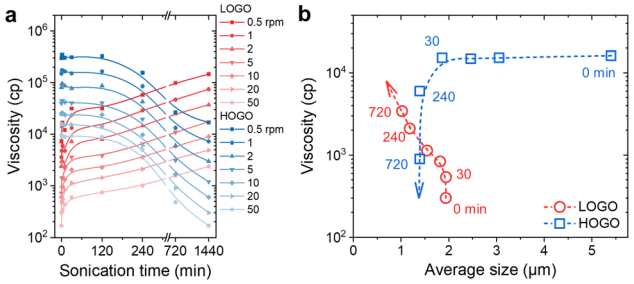

Fig. 3 Opposite viscoelastic evolution of LOGO and HOGO under ultrasonic fragmentation. (a) Steady state viscosity of LOGO and HOGO sonicated for different times measured with a wide range of spindle rotational speed (0.5–50 rpm). (b) Evolution of viscosity of GO dispersion at a fixed spindle rotational speed (20 rpm) depending on the average size of GO nanosheets for LOGO and HOGO under ultrasonic fragmentation.

Consequently, both LOGO and HOGO exhibited analogous fragmentation behaviors under ultrasonication, with the primary distinction being their initial sizes. To minimize thermal effect on their chemical composition, as well as the occurrence of structural defects due to ultrasonication, we conducted this study using bath sonication rather than tip sonication.[34] Importantly, our analysis revealed no significant chemical changes during sonication, as evidenced by the negligible change in the infrared absorption spectra observed through FTIR spectroscopy (Fig. 2d).

Opposite viscoelastic evolution of LOGO and HOGO

Interestingly, despite exhibiting similar fragmentation behavior, LOGO and HOGO displayed contrasting rheological evolution under ultrasonication. Both LOGO and HOGO, in line with typical GO dispersions, exhibited shear-thinning behavior with decreasing viscosity as the spindle rotation speed increased, following a power-law relationship as shown in Fig. S2.[12]† However, as shown in Fig. 3a, the trend in viscosity changes due to fragmentation revealed opposing behaviors between LOGO and HOGO. In the early stage (<30 min), viscosity of LOGO drastically increased and a more gradual increase in viscosity was continuously observed until 1440 min. On the other hand, viscosity of HOGO is comparably constant in the early stage of the sonication (<30 min) and then continuously decreased.

The increase in viscosity of LOGO attributed to sonication has been previously interpreted as the formation of fracture-induced gelation, where the generation of fresh edges enhances inter-sheet interactions, ultimately leading to the formation of a three-dimensional (3D) network.[22] The formation of a 3D network through gelation was supported by imaging freeze-dried LOGO structures (Fig. S3†). After 120 min of sonication, lyophilized LOGO shows a periodic and ordered structure, which typically appears in lyophilized GO hydrogels.[17,22,38] The more magnified images for 120-min sonicated LOGO revealed regions where the edges of sheets appear to be connected, whereas the LOGO before sonication doesn't exhibit such features. Conversely, HOGO did not exhibit an increase in viscosity due to gelation under the same sonication conditions; instead, it showed a tendency for viscosity to decrease. This can be explained from the perspective of the excluded volume. Theoretically, for freely rotating disk-shaped particles with a diameter of D and a particle number density of ρ, the excluded volume fraction is $\rho\pi D^3/6$.[39] If a GO sheet with an initial length of D is divided into N equal parts, reducing the sheet size to $D/\sqrt{N}$, the total exclusive volume fraction for all N particles decreases to $1/\sqrt{N}$ of that of the initial sheet. This indicates a reduced opportunity for inter-sheet interactions after fragmentation, leading to a decrease in viscosity. The initial plateau in HOGO's viscosity can be attributed to its highly liquid crystalline nature, as confirmed by POM observations (Fig. S4†). The marked reduction in birefringence after 30 min of ultrasonic treatment serves as evidence that the HOGO dispersion exhibits liquid crystalline characteristics in the early stages of sonication. In a liquid crystal state, GO nanosheets are highly arrested, limiting their free rotation. Consequently, even with fragmentation, the excluded volume experiences minimal change when compared to the isotropic phase, in which the exclusive volume of GO nanosheets is highly size-dependent as described above. At least in our range of ultrasonication periods (<24 hours), LOGO and HOGO consistently exhibit divergent viscosity trends. More interestingly, as illustrated in Fig. 3b, the contrasting rheological evolution persists regardless of nanosheet size, even when the size of HOGO gets smaller to be less than the initial size of LOGO. The contrasting rheological behavior between LOGO and HOGO under fragmentation can be attributed to differences in their chemical composition, rather than their morphology.

Effect of electrostatic interaction on viscoelastic evolution of GO under ultrasonic fragmentation

To elucidate the underlying mechanism for the contrasting rheological responses of LOGO and HOGO during

ultrasonication, we investigated the influence of electrostatic interactions among GO sheets on their rheological behavior, drawing inspiration from the significant disparity in zeta potential between LOGO and HOGO. Previous studies have shown that GO gelation can be controlled by adjusting the electrostatic forces among GO sheets, either by modulating pH or ionic strength.[11,40,41] We adjusted the zeta potential and Debye length of HOGO by adding NaCl (Fig. 4a and b). According to the Gouy–Chapman model, Debye length is proportional to the inverse square root of ionic strength.[42,43] Therefore, an increase in ionic strength due to ion addition leads to a decrease in the absolute value of the zeta potential and Debye length.[44,45] The measured zeta potential of HOGO dispersion showed a decreasing trend in the absolute value as ionic strength increased, and at 50 mM and beyond, the zeta potential of HOGO could be adjusted to a level similar to that of LOGO.

The viscosity of HOGO undergoing sonication at different ionic strengths is presented in Fig. 4c. At an ionic strength of 50 mM, there was a reduction in the rate of viscosity decrease compared to neat HOGO, but a significant increase in viscosity like in LOGO was not observed. In contrast, when the ionic strength was 100 mM, viscosity showed an increase up to 120 minutes, similar to LOGO. This implies that fragmentation-induced gelation could also occur in NaCl-added HOGO where electrostatic repulsion between GO sheets is weakened. We should note that, to independently investigate the influence of zeta potential on gelation behavior, we limited our experimental range to ionic strengths that had a minimal impact on viscosity before fragmentation (Fig. 4c, inset). Up to 100 mM, initial viscosity remained relatively stable, but at 200 mM, we observed a rapid increase in initial viscosity accompanied by the appearance of visible aggregation of GO.

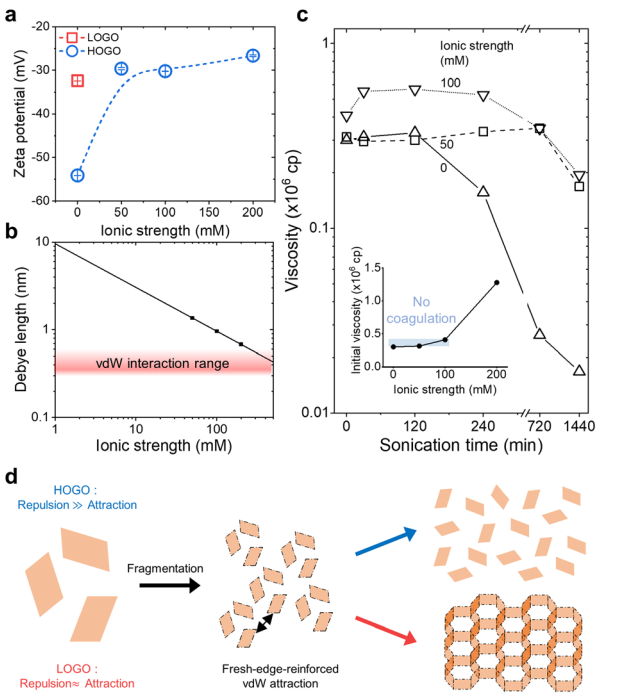

Fig. 4 Exploring the fragmentation-induced gelation regime of HOGO by adding salt. (a) Zeta-potential measured by ELS depending on the NaCl concentration. (b) Estimated Debye length as a function of the ionic strength of the dispersion, calculated using the Gouy–Chapman model. The typical range of van der Waals (vdW) interaction distances is shaded in red. (c) Viscosity evolution of HOGO with different ionic strengths under ultrasonic treatment. The inset graph shows initial viscosity before sonication depending on ionic strength where the range of the experiment is marked by a blue shadow. The spindle rotational speed was fixed at 0.5 rpm. (d) Proposed mechanism for distinctive viscoelastic evolution of graphene oxide depending on electrostatic repulsion between GO nanosheets.

These findings collectively indicate that GO dispersions undergo fragmentation-induced gelation when the zeta potential approximates −30 mV. Beyond this threshold, the dispersions become unstable, leading to coagulation. This critical zeta potential represents a delicate equilibrium point where electrostatic repulsion and van der Waals attraction are finely balanced. As depicted in Fig. 4d, when GO dispersions maintain this delicate balance between attractive and repulsive forces, the process of fragmentation-induced fresh-edge formation strengthens attractive forces, ultimately resulting in the gelation of graphene oxide. Conversely, when electrostatic repulsion prevails, the reinforcement of attractive forces is insufficient to induce gelation, leading to decreased viscosity due to the reduced excluded volume of freely rotating smaller GO nanosheets. In terms of interaction range, gelation exclusively occurs when the Debye length is comparable with the range of van der Waals interactions, while fresh-edge-induced gelation remains unattainable when the Debye length significantly surpasses the extent of attractive forces.

To investigate the transition in viscoelastic behavior of HOGO under sonication with the addition of salt, we conducted rheological measurements using the frequency sweep method for neat HOGO and HOGO with 100 mM NaCl, both before and after sonication (Fig. 5). G' and G'' represent the elastic and viscous characteristics of the GO network, respectively. For neat GO, G' at low frequency (0.1 rad per s) decreases after sonication (Fig. 5a). In contrast, when 100 mM of salt was added to weaken the repulsive forces, G' increased with sonication (Fig. 5d). For neat GO, the slope of G' becomes steeper after sonication, indicating a more significant reduction in elasticity. However, for salt-added GO, the slope was flattened after sonication. These observations, along with the respective decrease and increase in the low-frequency elastic modulus, as well as the corresponding changes in gel-like frequency independence,[46] confirm that electrostatic screening due to the addition of salt influences fragmentation-induced gelation during sonication. This reinforces the understanding that electrostatic interactions play a crucial role in the viscoelastic properties of GO under sonication. The G'/G'' ratio also indicates how gel-like the GO dispersion is.[47] After sonication, neat HOGO becomes more liquid-like in all frequency regions (Fig. 5b and c), whereas HOGO with 100 mM NaCl shows a significant increase in G'/G'' in the low frequency region, indicating enhanced gel-like properties (Fig. 5e and f). However, in the high frequency regime, G'/G'' decreases, suggesting that the network may collapse under shear, exhibiting weak gel characteristics. Overall, the rheological analysis supports our proposed

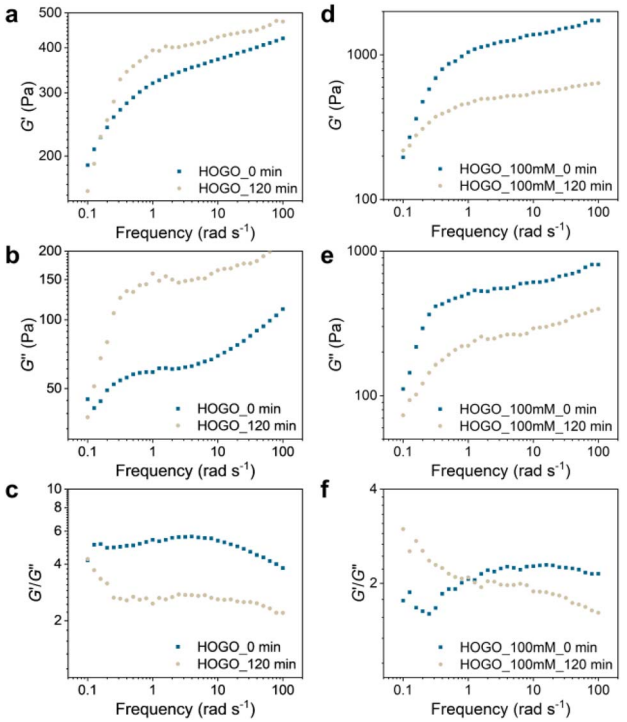

Fig. 5 Dynamic frequency sweep of neat HOGO and 100 mM NaCl-added HOGO performed at a constant strain of 1%. Panels (a–c) show G', G'', and G'/G'' as functions of frequency for neat HOGO, while panels (d–f) present the corresponding data for HOGO with 100 mM NaCl. Blue dots represent data before sonication, and ivory dots represent data after 120 minutes of sonication for each GO dispersion.

mechanism of fragmentation-induced gelation, which occurs only when the repulsive forces are weakened.

Conclusions

In conclusion, this study elucidates the pivotal role of electrostatic interactions in the rheological evolution of GO dispersions under ultrasonication. The significant disparity between the electrostatic repulsion force in HOGO and that in LOGO has emerged as a key determinant in the occurrence of fragmentation-induced gelation. By altering the ionic strength and consequently the zeta potential and Debye length of HOGO, we demonstrate that controlled electrostatic repulsion can shift the balance, making fragmentation-induced gelation feasible. Specifically, our findings indicate that GO dispersions exhibit gelation behavior when the zeta potential approximates −30 mV, where electrostatic repulsion and van der Waals attraction delicately balance. This study not only provides valuable insights into the manipulation of GO's rheological properties, essential for tailoring its suitability for a wide range of applications, but also sheds light on long-standing contradictions in previous research regarding the rheological evolution of GO under sonication.

Data availability

Data for this article, including dataset for figures are available at Figshare at **https://doi.org/10.6084/m9.figshare.26112604**.

Author contributions

Dongpyo Hong: conceptualization, formal analysis, investigation, methodology, validation, visualization, writing – original draft, writing – review & editing. Matlabjon Sattorov: investigation, writing – review & editing. Ok Sung Jeon: investigation, writing – review & editing. Se Hun Lee: validation, writing – review & editing. Gun-Sik Park: conceptualization, resources, writing – review & editing, Young Joon Yoo: conceptualization, writing – review & editing. Sang Yoon Park: conceptualization, funding acquisition, project administration, resources, supervision, writing – review & editing.

Conflicts of interest

The authors declare that they have no competing interests.

Acknowledgements

This research was supported by the Nano-Material Technology Development Program through the National Research Foundation of Korea (NRF) funded by the Ministry of Science and ICT (No. 2018M3A7B4070990), the National Research Foundation of Korea (NRF) grant funded by the Korea Government (MSIT) (No. 2016R1A3B1908336, 2020R1A2C2103137, 2020R1F1A1076359 and 2022R1C1C2011696), the Technology Innovation Program funded by the Ministry of Trade, Industry & Energy (MI, Korea) (No. 20020216-K_G012002021601-10054408 and RS-2023-00236794), and the "Gyeonggi-do Tested Utilization Semiconductor Technology Development Project" managed by the Advanced Institute of Convergence Technology with financial resources from Gyeonggi-do in year 2023 (AICT-06TB2).

References

1 D. Li, M. B. Muller, S. Gilje, R. B. Kaner and G. G. Wallace, *Nat. Nanotechnol.*, 2008, **3**, 101–105.
2 D. A. Dikin, S. Stankovich, E. J. Zimney, R. D. Piner, G. H. Dommett, G. Evmenenko, S. T. Nguyen and R. S. Ruoff, *Nature*, 2007, **448**, 457–460.
3 H. Liu, H. Wang and X. Zhang, *Adv. Mater.*, 2015, **27**, 249–254.
4 A. Akbari, P. Sheath, S. T. Martin, D. B. Shinde, M. Shaibani, P. C. Banerjee, R. Tkacz, D. Bhattacharyya and M. Majumder, *Nat. Commun.*, 2016, **7**, 10891.
5 L. Peng, Z. Xu, Z. Liu, Y. Guo, P. Li and C. Gao, *Adv. Mater.*, 2017, **29**, 1700589.
6 Z. Xu, Z. Liu, H. Sun and C. Gao, *Adv. Mater.*, 2013, **25**, 3249–3253.
7 G. Xin, T. Yao, H. Sun, S. M. Scott, D. Shao, G. Wang and J. Lian, *Science*, 2015, **349**, 1083–1087.
8 Z. Xu, Y. Liu, X. Zhao, L. Peng, H. Sun, Y. Xu, X. Ren, C. Jin, P. Xu, M. Wang and C. Gao, *Adv. Mater.*, 2016, **28**, 6449–6456.
9 J. Yan, Y. Leng, Y. Guo, G. Wang, H. Gong, P. Guo, P.-H. Tan, Y.-Z. Long, X. Liu and W.-P. Han, *ACS Appl. Mater. Interfaces*, 2019, **11**, 10810–10817.

10 L. Li, Y. Guo, X. Zhang and Y. Song, *J. Mater. Chem. A*, 2014, **2**, 19095–19101.
11 H. Bai, C. Li, X. Wang and G. Shi, *J. Mater. Chem. C*, 2011, **115**, 5545–5551.
12 Z. Xu and C. Gao, *ACS Nano*, 2011, **5**, 2908–2915.
13 P. Kumar, U. N. Maiti, K. E. Lee and S. O. Kim, *Carbon*, 2014, **80**, 453–461.
14 C. Vallés, R. J. Young, D. J. Lomax and I. A. Kinloch, *J. Mater. Sci.*, 2014, **49**, 6311–6320.
15 M. Zhang, Y. Wang, L. Huang, Z. Xu, C. Li and G. Shi, *Adv. Mater.*, 2015, **27**, 6708–6713.
16 C. Luo, W. Lv, C. Qi, L. Zhong, Z.-Z. Pan, J. Li, F. Kang and Q.-H. Yang, *Adv. Mater.*, 2019, **31**, 1805075.
17 K. C. Wasalathilake, D. G. D. Galpaya, G. A. Ayoko and C. Yan, *Carbon*, 2018, **137**, 282–290.
18 B. Bahaya, D. Johnson and C. Yavuzturk, *J. Heat Transfer*, 2018, **140**, 064501.
19 B. Zhang and T. Chen, *Materials*, 2019, **12**, 1757.
20 A. Ansón-Casaos, J. C. Ciria, O. Sanahuja-Parejo, S. Víctor-Román, J. M. González-Domínguez, E. García-Bordejé, A. M. Benito and W. K. Maser, *Phys. Chem. Chem. Phys.*, 2020, **22**, 11474–11484.
21 I. Malnarič, B. Alič, M. Krajnc, A. Vesel and U. Šebenik, *Colloids Surf.*, 2023, **675**, 132012.
22 O. C. Compton, Z. An, K. W. Putz, B. J. Hong, B. G. Hauser, L. Catherine Brinson and S. T. Nguyen, *Carbon*, 2012, **50**, 3399–3406.
23 A. Ojha, H. Ibrahim, N. Alyabyeva, R. Lazzari, M. Goldmann and P. Thareja, *Synth. Met.*, 2020, **269**, 116494.
24 M. Sandhya, D. Ramasamy, K. Sudhakar, K. Kadirgama and W. Harun, *Ultrason. Sonochem.*, 2021, **73**, 105479.
25 J. Lin, P. Li, Y. Liu, Z. Wang, Y. Wang, X. Ming, C. Gao and Z. Xu, *ACS Nano*, 2021, **15**, 4824–4832.
26 M. P. Araújo, O. Soares, A. Fernandes, M. Pereira and C. Freire, *RSC Adv.*, 2017, **7**, 14290–14301.
27 T. Chen, B. Zeng, J. Liu, J. Dong, X. Liu, Z. Wu, X. Yang and Z. Li, *J. Phys.: Conf. Ser.*, 2009, **188**, 012051.
28 L. Sun and B. Fugetsu, *Mater. Lett.*, 2013, **109**, 207–210.
29 A. Ganguly, S. Sharma, P. Papakonstantinou and J. Hamilton, *J. Mater. Chem. C*, 2011, **115**, 17009–17019.
30 R. Larciprete, S. Fabris, T. Sun, P. Lacovig, A. Baraldi and S. Lizzit, *J. Am. Chem. Soc.*, 2011, **133**, 17315–17321.
31 A. Kovtun, D. Jones, S. Dell'Elce, E. Treossi, A. Liscio and V. Palermo, *Carbon*, 2019, **143**, 268–275.
32 S. Pan and I. A. Aksay, *ACS Nano*, 2011, **5**, 4073–4083.
33 S. Ye and J. Feng, *RSC Adv.*, 2016, **6**, 39681–39687.
34 C. Mellado, T. Figueroa, R. Baez, M. Melendrez and K. Fernandez, *Mater. Today Chem.*, 2019, **13**, 1–7.
35 C. Cai, N. Sang, Z. Shen and X. Zhao, *J. Exp. Nanosci.*, 2017, **12**, 247–262.
36 K. Kouroupis-Agalou, A. Liscio, E. Treossi, L. Ortolani, V. Morandi, N. M. Pugno and V. Palermo, *Nanoscale*, 2014, **6**, 5926–5933.
37 G. Gonçalves, M. Vila, I. Bdikin, A. De Andrés, N. Emami, R. A. Ferreira, L. D. Carlos, J. Grácio and P. A. Marques, *Sci. Rep.*, 2014, **4**, 6735.
38 Y. Shao, M. F. El-Kady, C. W. Lin, G. Zhu, K. L. Marsh, J. Y. Hwang, Q. Zhang, Y. Li, H. Wang and R. B. Kaner, *Adv. Mater.*, 2016, **28**, 6719–6726.
39 S. Jogun and C. Zukoski, *J. Rheol.*, 1999, **43**, 847–871.
40 X. Yang, L. Qiu, C. Cheng, Y. Wu, Z. F. Ma and D. Li, *Angew. Chem., Int. Ed.*, 2011, **50**, 7325–7328.
41 G. Liao, J. Hu, Z. Chen, R. Zhang, G. Wang, T. Kuang and L. Zhang, *Front. Chem.*, 2018, **6**, 450.
42 J. C. Berg, *An Introduction to Interfaces & Colloids: the Bridge to Nanoscience*, World Scientific, 2010.
43 M. Khademi and D. P. Barz, *Langmuir*, 2020, **36**, 4250–4260.
44 B. Konkena and S. Vasudevan, *J. Mater. Chem. C*, 2014, **118**, 21706–21713.
45 W. B. Russel, W. Russel, D. A. Saville and W. R. Schowalter, *Colloidal Dispersions*, Cambridge university press, 1991.
46 C. Vallés, *Graphene Oxide: Fundamentals and Applications*, 2016, pp. 121–146.
47 S. Naficy, R. Jalili, S. H. Aboutalebi, R. A. Gorkin III, K. Konstantinov, P. C. Innis, G. M. Spinks, P. Poulin and G. G. Wallace, *Mater. Horiz.*, 2014, **1**, 326–331.